Optimization of a Thermoelectric IR-Detector for Low Working Temperature

R. Fettig, H.-J.Lerchenmüller, E. Müller

Universität Karlsruhe, Institut für Angewandte Physik, Germany

Abstract

Thermoelectric IR-detectors have been developed for working at a temperature of 170 K in the CIRS experiment of the designated interplanetary CASSINI mission. Thermoelectric legs of p- and n-type are soldered isolated one from another to a metallized ceramic substrate. Pyramidal legs are formed by electric discharge machining (EDM). A thin gold foil is welded to the cones and blackened for high absorption of radiation. Characterization measurements are carried out to correlate detector properties with the influence of preparation process and material used. Thermoelectric behaviour is described by measuring the current-voltage-characteristics from liquid nitrogen up to room temperature. Material of various composition within the pseudobinary systems Bi_2Te_3-Sb_2Te_3 (for p-type) and Bi_2Te_3-Bi_2Se_3 (for n-type) has been used for detector preparation. By choosing material of proper doping the maximum of the figure of merit could be shifted towards lower temperatures.

1 Introduction

Thermoelectric detectors along with Golay-cells, bolometers and pyroelectric detectors belong to the most sensitive thermal IR sensors. Their construction principle is simple, they don't require any external voltage supply and exhibit a constant responsivity over a wide spectral range, an appropriate absorber provided.
Detectors of the Hilgert-Schwarz-type [1] have been built using highly effective thermoelectric material on the basis of $(Bi_{1-x}Sb_x)_2(Te_{1-y}Se_y)_3$. [2, 3]. Detectors have been built which showed below 200 K a specific detectivity up to $5 \cdot 10^9\ cm\sqrt{Hz}/W$ at a response time of about 40 ms [4].

Because of the high performance figures and the simple construction and operation, these thermoelectric detectors have been designated for application within the Composite Infrared Spectrometer Experiment (CIRS) of the interplanetary CASSINI mission of NASA and ESA. CASSINI, scheduled to be launched in 1997 as a successive mission of Voyager II, is expected to provide enhanced information of IR emission of Saturn and its moon Titan towards the far infrared.

The mission objectives, specify the detector requirements as follows:

- A specific detectivity: $D^* \geq 4 \cdot 10^9 cm\sqrt{Hz}/W$
- Modulation frequencies up to 26 Hz, response time $\tau \leq 40$ ms
- Working temperature: 170 K
- Maximal absorption in the spectral range from mid to far infrared (15..1000 μm)
- Operated as a current source with a successive transformer
- A detector resistance $R_{el} \geq 5\ \Omega$ at 170 K
- Low geometric tolerances, long life time, cleanliness, stability against acceleration and vibration as well as against temperature variation

That requires on the one hand an optimization of the detector properties with respect to material and technology, on the other hand concentration on reliability and reproducibility of the results.

2 Fundamental

Fig. 1 demonstrates the function principle of the detector: An absorbing structure is heated by radiation, its temperature is measured by a thermoelement.The construction geometry in the presented way is referred to as Hilger-Schwarz-type: A thin freestanding metal foil serves as the substrate for the absorbing structure. It provides a thermal connection between the absorbing areas and the thermoelectric legs and as electric bridge of the thermoelement. The metal foil is linked to the two legs of thermoelectric p- and n-type materials via contact areas of a few μm in diameter. The legs are electrically isolated one from another and thermally connected to a heat sink of ambient temperature. For achieving maximal DC-responsivity heat losses from the absorber by a surrounding gas has to be avoided, therefore the system is working in vacuum.

The distribution of electric and thermal currents through the detector are represented by the electric and thermal circuit diagrams (Fig. 2).
Electrically the detector can be considered as a source of voltage with an internal resistance, which consists in the ideal case of the sum of the leg resistances $R_{ec}^{p;n}$. For the real detector contact resistances $R_{ek}^{1,2}$ have to be added.
Thermally the sensor represents a thermal relaxator: The absorbing structure possesses a heat capacity C_w and is thermally coupled to surroundings by heat conduction through the legs ($R_{wc}^{p;n}$) and thermal radiation (R_{wr}). Upon irradiation, the temperature of the absorber rises. If in addition an electric current flows through the thermoelement, the temperature of the cone tips is altered due to the combined effect of Peltier effect, Thomson effect and Joule heating. The latter ones can be described to be conducted half by half towards the absorber and into surroundings [5]. Additional Joule heat $P_{ejk}^{1,2}$ is released on the electric contact resistances.

The ring-shaped narrow passage through the foil around the contact points represents a thermal contact resistance. Thermal by-passes R_{wb} due to electrically poor conducting parallel contacts between foil and material have to be suggested. The relaxation behaviour is defined by the heat capacity of the absorbing structure as well as by the heat resistance due to conduction via the thermoelement and radiation.
The detection limit of the sensor is determined by the magnitude of noise voltage (see Table 1) [6]. Johnson noise is the dominating mechanism, however at high values of the figure of merit the influence of temperature fluctuations becomes relevant. During low frequency AC-operation with DC-offset to the signal 1/f-noise is appreciable. This can be suppressed by a special compensation circuit formed out of two identical detectors. Current noise is insignificantly small and can be ignored.

For manufacturing cubes of thermoelectric material (edge length about 500 μm) are soldered to a ceramic carrier of Al_2O_3 coated with a structured nickel layer (Fig. 3). The cubes are then shaped into cones or pyramides($\approx$ 150 μm edge length, top area $\approx 10 \times 10\ \mu m^2$) by EDM. [3]. A 100 nm thick gold foil with an area of about 1 mm^2 (mass about 2 μg) is welded onto the tips. A layer of gold black of about 10 μm in thickness is evaporated in inert atmosphere of several mbar onto the foil as absorber layer [7, 8].

The following detector parameters have been measured with an automated apparatus [4] between room temperature and liquid nitrogen tempe-

rature, for blackenend as well as for unblackened detectors and are listed in table 1:

- Responsivity (r) at room temperature: The detector is irradiated by an calibrated halogen lamp through a quartz window and the detector voltage is measured. Because of the strong spectral dependence of absorption by gold in the visible, responsivity values for unblackened sensors can only be compared for equal irradiation conditions.
- Responsivity below room temperature: Irradiation is performed by a calibrated LED, which is cooled down together with the detector, so that an offset to the signal due to background radiation is avoided.
- Response time (τ) : Assuming that the detectors relaxation behaviour can be described by a thermal low-pass, the time constant of the exponential curve of response to a step function is determined.
- Electrical resistance (R_{el}): At a frequency of 8 kHz a four-point measurement is carried out.
- Characterization of the detector as a thermoelement is achieved by determination of the current-voltage-characteristics. The fraction U/I contains the electric resistance R_{el} and an additional current dependent portion. It is related to the thermo-e.m.f. due to the temperature difference between absorber and surroundings caused by Peltier-effect, Thomson-effect and Joule heat. This shall here be referred to as Peltier-resistance R_p. From the relation of its value for $I \rightarrow 0$ (R_{p0}) to the electrical resistance $R_{p0}/R_{el} = z_{eff}T$ the figure of merit z_{eff} of the thermoelement is obtained.

For computation of specific detectivity theoretical noise values of temperature fluctuations and Johnson noise have been taken into consideration. From the ratio of measured responsivities of a detector before and after blackening the specific emissivity of the unblackened sensor can be computed. The comparison of response times at low temperatures allows for the estimation of the mass of the deposited gold black.

3 Detector Optimization - Technology and Material

There are number of possibilities for affecting the detector properties by technological factors: The smallest possible thickness of gold foil is given by mechanical stability requirements, that for the absorber layer by the necessary absorption in the far infrared. From this results a lower limit to the heat capacity of the absorbing structure. Hence, the response time can only be lowered by reducing the heat conduction resistance. This can be done by varying the size of the contact area and the opening angle of the pyramidal tips. A lowering of the heat conduction resistance leads to faster detectors, with the influence of a constant contact resistance increasing. The geometrical resistance of the foil, which decreases logarithmically with rising contact diameter, gains of relevance. Contact resistances are inversely proportional to area and are therefore independent of the contact dimensions.

Theoretically the welding energy for fixing the foil is high enough to melt a sample region, in which the main fraction of temperature difference between absorber system and surroundings is concentrated and where the main part of the signal is generated. An increase of the specific detectivity at low temperatures could be expected if application of a soldering method for foil fixing was managed.
For improving the contact's mechanical stability the gold foil can be covered with small spots of BiSn-solder near the contact region. Otherwise a depletion of the welding connection may occur due to corrosive processes which may lead to the destruction of the contact.

The influence of the EDM process on the Seebeck-coefficient at the material surface was also investigated. For this purpose, two neighbouring areas on a surface have been processed using two different values of current. With a locally resolved measurement of the Seebeck-coefficient [9] a line-scan was drawn over both areas (see Fig. 5). At the same time an altitude profile of the scan was recorded, which makes visible the border line of the areas slightly inclined one to another. For the p-type as well as for the n-type material a significant lowering of the absolute value of the Seebeck-coefficient was found at a higher rate of EDM current, while it remained nearly unaltered after processing with the lowest possible current stress. A striking effect is the stronger degradation near the edge at the border line between both areas. From a thermo-probe measurement in unsteady state an integral information over sample regions reaching different depths is obtained [10]. With increasing depth only a slight shift towards the bulk value was observed. This implies, that the surface layer with reduced Seebeck-coefficient is of thickness comparable to the penetration depth in the steady state, which is of the order of 10 μm. SEM-images of EDM-processed surfaces of our thermoelectric material shows structures of finegrained solidified material with sizes of several μm.
The fact that near the edges thermoelectric material is modified more strongly than on plane areas can be explained as a result of the concentration of electric field near the material edges during EDM as well as due to the geometrically constrained heat transport away from these regions. This is of interest, because the contact area between the leg and the foil is situated in the immediate neighbourhood of the convex EDM edges.

A change of the carrier density in the degraded surface layer, possibly induced by a decrease of tellurium contents, should shift the Seebeck-coefficient for material of different conduction types into opposite directions. This is thought to arise due to the influence of the fine-crystalline structure in the degraded surface layer on carrier scattering. Model computations on the effect of grain boundary scattering on thermoelectric properties [11] showed, that the Seebeck-coefficient reacts sensitively to a high contents of grain boundaries. Under certain conditions of grain size and scattering potential it may be significantly lowered.
Assuming, that p- and n-leg possess equal thermoelectric properties per absolute value and by restricting to Johnson noise and temperature fluctuations the specific detectivity of the real thermoelectric detector can be derived from the specific detectivity of the ideal thermal detector $D^*_{id} = \epsilon/\sqrt{16 k_B \sigma_S T^5}$ [6] by introducing factors describing the effect of thermal and electric contact resistances R_{wk}, R_{ek} in a way that only the specific emissivity ϵ and the figure of merit of the thermoelectric material zT are introduced:

$$D^* = \sqrt{\frac{\epsilon f_w f_e zT}{1+f_w f_e zT}} \sqrt{f_r} D^*_{id}, \qquad (1)$$

where

$$f_r = (1 + \frac{R_{wk}+R_{wr}}{R_{wc}})^{-1} \qquad R_{wr} = \frac{1}{4\epsilon\sigma_S A T^3}$$

$$f_w = (1 + \frac{R_{wk}+R_{wc}}{R_{wr}})^{-1} \qquad f_e = (1 + \frac{R^{1,2}_{ek}}{R^{p,n}_{ec}})^{-1}$$

$$R_{wc} = R^{p,n}_{wc}/2 \qquad R_{wk} = R^{1,2}_{wk}/2$$

Considering the correction factors f_w und f_r yields, that D^* decreases for very small as well as for very large heat conduction resistances R_{wc}. A maximum value of D^* is found for a ratio of heat conduction resistance and radiation resistance $R_{wc}/R_{wr} = \sqrt{1+zTf_e}$. For vanishing thermal contact resistance, maximal absorption and the best thermoelectric material available ($zT \approx 1$) the maximal specific detectivity of the thermoelectric detector amounts $D^* \approx \sqrt{1/6} D^*_{id}$. It reduces with growing thermal contact resistances. Hence, if there are no additional requirements with respect to response time, the higher detectivity can be attained if the thermoelectric material with a figure of merit zT is optimized for the desired working temperature, the heat conduction resistance has been tuned to the optimal value with respect to the radiation resistance at the working temperature and a maximal absorption is reached.

In the present application a lower response time than that obtained by such a maximization is needed, and therefore requires a smaller heat conduction resistance. If two different materials of equal figure of merit are available (e.g. $Bi_{1-x}Sb_x$ and $Bi_2(Te_{1-y}Se_y)_3$ as n-type material near 150

K), the one with the smaller thermal conductivity should be chosen. In this way the contact area for a given heat resistance is larger and the area-dependent contact resistances are reduced. On the other hand, a large ratio of thermal to electrical conductivity of the material κ/σ is of advantage, because at a given heat resistance of the legs their electric resistance will be higher and hence the influence of electric contact resistances will be reduced.
Maximization temperature of the material's figure of merit has to be shifted from the working temperature of the detectors towards falling ratio κ/σ, i.e. to lower temperatures for both substances mentioned above . Because the maximum of the funtion $zT(T)$ of $(Bi_{1-x}Sb_x)_2(Te_{1-y}Se_y)_3$-compounds is relatively flat, D^* is only slightly lowered at working temperature however a reduction in the response time and an increase of κ/σ is achieved. The effect is higher, the more the temperature coefficients of electric and thermal conductivity of the material differ, i.e. the higher the contribution from lattice κ_G to the entire heat conductivity and the stronger the effects of bipolar thermal conductivity in a temperature range slightly above the maximum of zT.
The negative influence of electrical and thermal contact resistances will be amplified by the deviation from resistance value for maximal detectivity due to reduction of response time. The factors f_ω and f_c (see (1)), which are limiting D^* are increasingly determined by the contact resistances. Contact resistances with low or negative temperature coefficients are especially harmful for low-temperature applications, because their influence increases with falling temperature. In this way it can be explained, why towards the lower temperatures the theoretically expected strong increase of specific detectivity has not been measured yet. The formation of oxide contact resistances with such temperature coefficients may be caused during the welding of the foils.

Therefore the replacement of $Bi_2(Te_{1-y}Se_y)_3$ by $Bi_{1-x}Sb_x$ with its higher thermal conductivity will only be useful if $Bi_{1-x}Sb_x$ shows a significantly higher figure of merit.

The figure of merit z of a thermoelectric material depends on the composition and the position of the reduced Fermi level [12]. Crucial for the choice is the maximization parameter $\mu_o\ m_d^{3/2}/\kappa_G$ (m_d - density of states mass, κ_G - lattice thermal conductivity, μ_o - carrier mobility for non-degenerated case). The lowest values of κ_G within the pseudobinary system bismuth telluride-antimony telluride was found near $(Bi_{0.5}Sb_{0.5})_2Te_3$ [13]. P-type material of the constitution $(Bi_{0.25}Sb_{0.75})_2Te_3$ which is preferred for room temperature applications (referred to as standard material) has a significantly higher value $\mu_o\ m_d^{3/2}$ compared to $(Bi_{0.5}Sb_{0.5})_2Te_3$ at 300 K [12]. However, at lower temperatures $(Bi_{0.5}Sb_{0.5})_2Te_3$ is more favourably disposed. [14]. Below 150..200 K $(Bi_{0.5}Sb_{0.5})_2Te_3$ exhibits the better properties. If the carrier density is lowered in comparison to room temperature optimized material, the thermoelectric properties worsen at room temperature, but at lower temperatures zT rises. The temperature dependence shifts its maximum towards lower temperatures. The necessary carrier density reduction can be obtained merely by an increased contents of Te in growth for a composition near $(Bi_{0.5}Sb_{0.5})_2Te_3$, because the range of existence of the homogenious δ-phase contains the stochiometric composition. Hence, doping can be avoided, which can reduce the carrier mobility.
bulk-properties [15], in a first approach a correlation between

With respect to its preparative advances Czochralski-grown material has been used, which can be produced with high homogeinty [16]. It showes large single crystalline ranges, from which blocks for the forming of legs can be obtained simply by cleaving. Suitable material of low carrier density with the compositions $Bi_2(Te_{0.95}Se_{0.05})_3$ (n-type) and $(Bi_{0.4}Sb_{0.6})_2Te_3$ (p-type) was available. A square scan with the thermoprobe on thin slices of the thermoelectric material parallel to the crystallographic c-axis was performed at room temperature [10]. The slices have been sawed into strips perpendicular to the cleavage planes. The strips have been cleaved into single blocks. In this way the Seebeck-coefficient of each of the legs is known at room temperature.

In comparison with detectors from standard material those made from low temperature optimized material (LTM) showed modified temperature dependences at lower temperatures with increased values of r, D^* and z_{eff} (Fig. 4). For both materials several detectors have been manufactured. Typical detectors of each group have been chosen. Within the groups the properties varied due to manufacturing effects. In order to exclude an influence of different blackening unblackened detectors have been chosen for comparison.

4 Model computations

Model equations of the temperature dependences of responsivity, specific detectivity, response time, electric resistance, figure of merit and first derivative of Peltier resistance have been formulated with the assumption of equal absolute values of the material properties of p- and n-type and contact resistances [15]. For a set of detectors made from a different batch of standard material and gold foils with solder spots theoretical curves could be fitted well by choosing appropriate values the following set of parameters:

- Thermopower of the thermoelement at room temperature and its temperature coefficient
- Temperature coefficient of electric conductivity of the leg material
- Ratio of thermal and electrical conductivity of the leg material as well as for the contact resistances at room temperature and temperature coefficient of both
- Ratio of contact resistance by leg resistance at room temperature.

The most important results obtained are: The model thermopower of the thermoelement reaches merely 60 % of the bulk value, independently of whether there have been used solder spots near the contacts or not. All temperature dependences of the model were found at a lower value than expected. The electrical contact resistance is at room temperature about 25 % of the leg resistance.

5 Conclusions

For optimization of fast thermoelectric IR-detectors for low temperatures with active material of $(Bi_{1-x}Sb_x)_2(Te_{1-y}Se_y)_3$ the requirement for maximal specific detectivity competes with the constraint of low response time. Therefore, a maximization of the figure of merit has to be achieved below working temperature.
The utilization of material of reduced carrier density yielded modified temperature dependences of responsivity, specific detectivity and figure of merit of the detectors, which form maxima below room temperature. A strong variation of detector characteristics caused by the manufacturing process was observed. Application of the material combination $(Bi_{0.5}Sb_{0.5})_2Te_3$-$Bi_{1-x}Sb_x$ seems promising.

A model fit for the interpretation of the measured temperature characteristics showed a notably reduced Seebeck-coefficient, which could be explained by the destruction of the monocrystalline structure of the thermoelectric material near the surface due to EDM or the welding process for foil fixing. It can be assumed, that a variety of grain boundaries are formed near the surface, which may reduce the Seebeck-coefficient. The injury of maximization condition as well as contact resistances limits the specific detectivity especially at low temperatures. An improvement of the detector performance can be expected by the application of soft shaping and fixing methods. Crucial for the detector's reliability is the stability of the connection between the legs and the foil.

Acknowledgements

The authors are very grateful to T.E. Svečnikova and L. D. Ivanova from Baikov-Institute of Metallurgy Moscow, GUS for providing Czochralski-grown single crystals. We are obliged to the group of Dr. H. Süßmann at Martin-Luther-Universität Halle/Wittenberg for performing of preparation procedures and thermo-probe measurements. The authors acknowledge NASA (NASW 4685) and DARA (50 OH 9202) for funding the project.

References

[1] Schwarz, E.
Britisch Patent Applications
57 81 87 and 87 81 88m, Research 5, 407 (1952)

[2] Richter, G.
Ein thermoelektrischer Infrarotdetektor.
Dissertation, Fakutät für Elektrotechnik, Universität Karlsruhe (1981)

[3] Fettig, R.; Balzer, M.; Birkholz, U.
Thermoelectric IR-Detectors.
8th Int. Conf. on Thermoel. Energy Conversion, Nancy, France 220-223 (1989)

[4] Fettig, R.; Birkholz, U.; May, M.
Temperature Depending Properties of Thermoelectric Infrared Detectors.
10th Int. Conf. on Thermoelectricity, Cardiff, Großbritannien (1991)

[5] Gehlhoff, P.O.; Justi, E.; Kohler, M.
Verfeinerte Theorie der elektrothermischen Kälteerzeugung.
Sammlung der Braunschweigischen Wissenschaftlichen Gesellschaft (1950)

[6] Smith, R.A.; Jones, F.E.; Chasmar, R.P.
The Detection and Measurement of Infra-Red Radiation.
Oxford Uni.Press,England (1957)

[7] Harris, L.
The optical properties of metal blacks and carbon blacks.
Monograph series No.1 Eppley Foundation f. Research) (1967)

[8] Bly, V.; Advena, D.J.; Cox, J.F.
The Deposition and Characterization of Far Infrared Absorbing Black Gold Films
Applied Optics, 32(7) 1136-1144 (1993)

[9] Süssman, H.; Syrowatka, S.; Reinshaus, P.
In: Transport in Verbindungshalbleitern
FB Physik, Martin-Luther-Universität Halle/Wittenberg (1989)

[10] Süßmann, H.; Bohm, M.; Reinshaus, P.
Scanning Thermo-Probe Technique - a Method for Determination of Concentration Profiles
12th Int. Conf. on Thermoelectrics, Yokohama, Japan (1993)

[11] Stordeur, M.
Charakterisierung und Optimierung thermoelektrischer Halbleiterschichten
Abschlußbericht zum DFG-Projekt (Az. 252/1-1)
FB Physik, Martin-Luther-Universität Halle/Wittenberg (1993)

[12] Stordeur, M.
Dissertation B
FB Physik, Martin-Luther-Universität Halle/Wittenberg (1985)

[13] Heiliger, W.
Dissertation A
FB Physik, Martin-Luther-Universität Halle/Wittenberg (1980)

[14] Müller, E.; Süßmann, H.; Baier, C.; Gaymann, A.; Ivanova, L. D.
Interpretation of Thermoelectric, Galvanomagnetic and Optical Properties of $(Bi_{1-x}Sb_x)_2Te_3$ mixed crystals within 100..300 K
12th Int. Conf. on Thermoelectrics, Yokohama, Japan (1993)

[15] Fettig, R.
Die Temperaturabhängigkeit der Kenngrößen thermoelektrischer Infrarotdetektoren
Dissertation, Fakultät für Physik, Universität Karlsruhe (1993)

[16] Svečnikova, T. E.; Ivanova, L. D.
private comunication

Figures

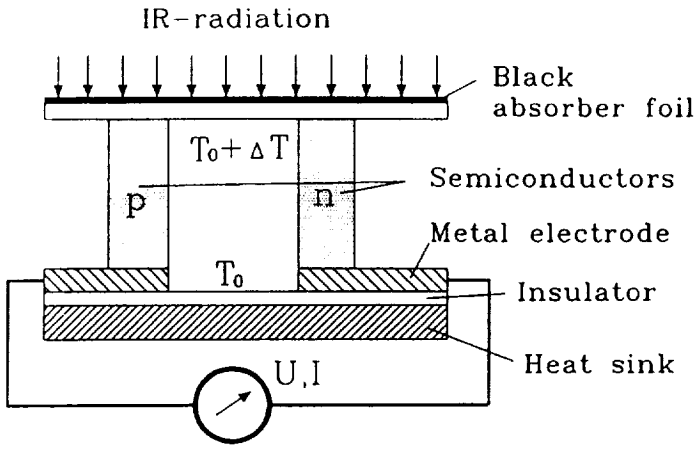

Figure 1
Principle of a thermoelectric infrared detector of the Hilger-Schwarz-type

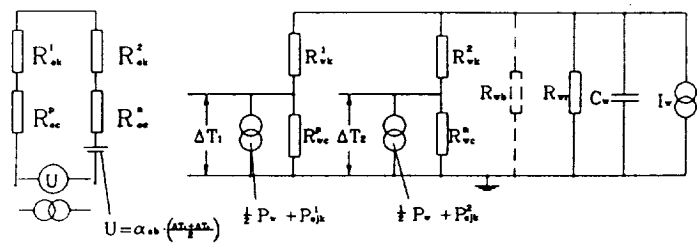

Figure 2
Electric and thermal circuit diagram of a real thermoelctric IR detector

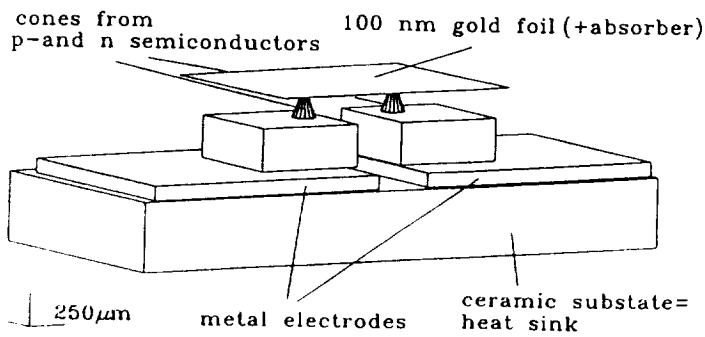

Figure 3
Scheme of a thermoelectric IR detector with cone geometry

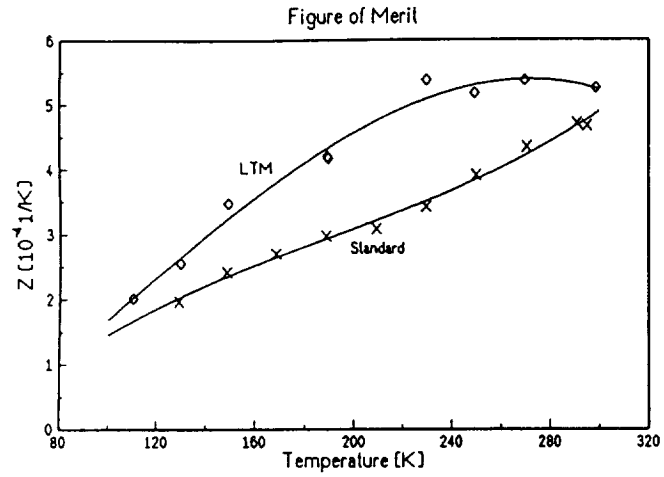

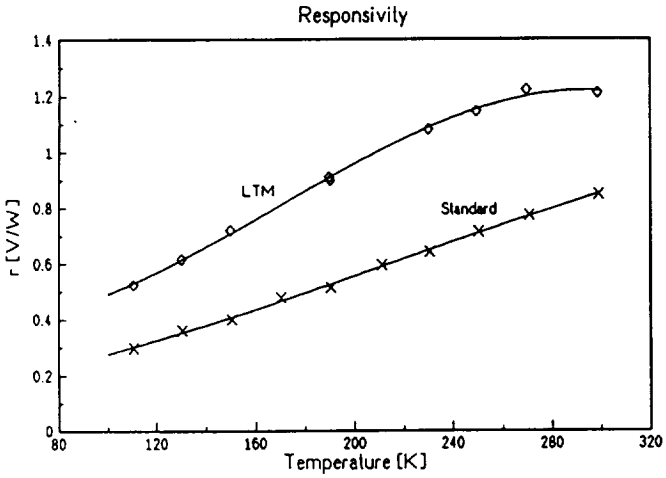

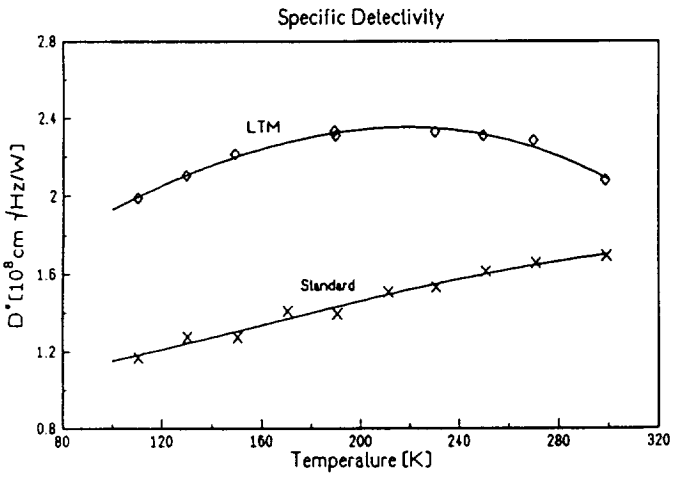

Figure 4
Temperature characteristics of figure of merit, responsivity and specific detectivity of unblackened detectors in comparison between standard material and low temperature optimized material (LTM)
Standard material
p-type: $(Bi_{0.25}Sb_{0.75})_2Te_3$
n-type: $(Bi_{0.95}Sb_{0.05})_2(Te_{0.95}Se_{0.05})_3$
LTM
p-type: $(Bi_{0.4}Sb_{0.6})_2Te_3$
n-type: $Bi_2(Te_{0.95}Se_{0.05})_3$

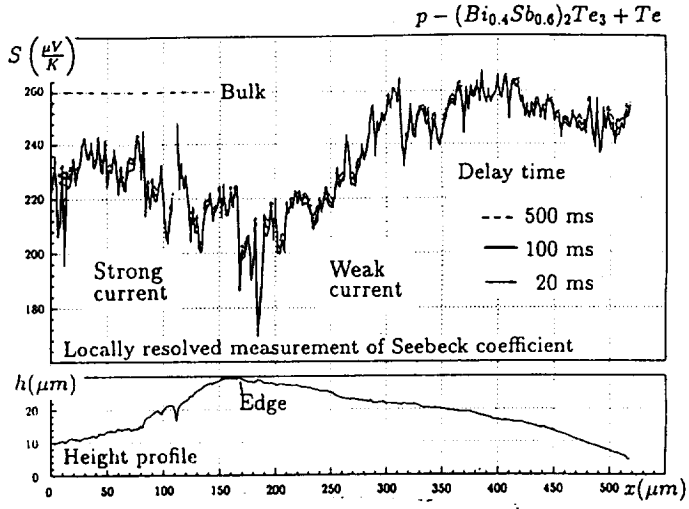

Figure 5
Line scan of the thermo-probe on a surface of thermoelectric material processed with electric discharge machining at different current magnitudes

Responsivity	r	=	$\frac{U_s}{I_\omega} = \frac{\alpha_{ab}\Delta T}{I_\omega} = \alpha_{ab}R^r_\omega \epsilon f(\nu)$	$\left[\frac{V}{W}\right]$
Noise voltage	U_n	=	$\sqrt{4k_BT\Delta\nu(R_{el} + \alpha^2_{ab}R^r_\omega T f(\nu))}$	[V]
Noise Equiv. Power	NEP	=	$\frac{U_n}{r}$	[W]
Specific detectivity	D^*	=	$\frac{(A\Delta\nu)^{1/2}}{NEP}$	$\left[\frac{cm\sqrt{Hz}}{W}\right]$
Response time	τ	=	$R^r_\omega C_\omega$	[s]
Current-voltage-characterisitics	$\frac{U}{I}$	=	$R_{el} + \frac{U_t(\Delta T)}{I} = R_{el0} + R_p$	
Peltier resistance $(I \to 0)$	R_{p0}	=	$\alpha^2_{ab}R^p_\omega T$	$[\Omega]$
	$\frac{dR_{p0}}{dI}$	~	$\alpha_{ab}R^p_\omega R_e$	$\left[\frac{\Omega}{A}\right]$

Table 1
Parameters for the description of a thermoelectric IR-detector with the signal voltage U_s, Boltzmann constant k_B, thermopower of the element α_{ab}, ν the measuring frequency and $\Delta\nu$ the measuring bandwidth, the absolute temperature T and the Area of the absorber A. R^r_ω, R^p_ω and R^I_ω are the different heat resistances relevant for the determination r, R_p and τ according to the thermal circuit diagram of figure 2.